First principle investigation of electronic structure, chemical bonding and optical properties of tetrabarium gallium trinitride oxide single crystal

ARTICLE *in* MATERIALS RESEARCH BULLETIN · MAY 2015

Impact Factor: 2.29 · DOI: 10.1016/j.materresbull.2015.04.064

2 AUTHORS:

Saleem Ayaz Khan

University of West Bohemia

38 PUBLICATIONS **123** CITATIONS

SEE PROFILE

Sikander Azam

University of West Bohemia

48 PUBLICATIONS **106** CITATIONS

SEE PROFILE

Materials Research Bulletin 70 (2015) 436–441

Contents lists available at ScienceDirect

Materials Research Bulletin

journal homepage: www.elsevier.com/locate/matresbu

First principle investigation of electronic structure, chemical bonding and optical properties of tetrabarium gallium trinitride oxide single crystal

Saleem Ayaz Khan *, Sikander Azam

New Technologies–Research Centre, University of West Bohemia, Univerzitni 8, 306 14 Pilsen, Czech Republic

ARTICLE INFO

Article history:
Received 14 February 2015
Received in revised form 28 April 2015
Accepted 30 April 2015
Available online 5 May 2015

Keywords:
Crystal structure
Semiconductivity
Charge-density waves
Electrical properties
Optical properties

ABSTRACT

The electronic band structure, valence electron charge density and optical susceptibilities of tetrabarium gallium trinitride (TGT) were calculated via first principle study. The electronic band structure calculation describes TGT as semiconductor having direct band gap of 1.38 eV. The valence electronic charge density contour verified the non-polar covalent nature of the bond. The absorption edge and first peak of dielectric tensor components showed electrons transition from N-p state to Ba-d state. The calculated uniaxial anisotropy (0.4842) and birefringence (−0.0061) of present paper is prearranged as follow the spectral components of the dielectric tensor. The first peak in energy loss function (ELOS) shows the energy loss of fast traveling electrons in the material. The first sharp peak produced in ELOS around 10.5 eV show plasmon loss having plasma frequencies 0.1536, 0.004 and 0.066 of dielectric tensor components. This plasmon loss also cause decrease in reflectivity spectra.

1. Introduction

The investigation of novel nitrides has become a rapidly growing field of interest for their unusual structures, high specific modulus (Si_3N_4), high thermal conductivity (AlN), emission of blue light (GaN) and superconducting (NbN) properties resilient mechanical strength and hardness (TiN) [1]. The unlike charges and chemical requirements of the anions of nitrogen and oxygen indicate that nitrides often reveal structural features totally dissimilar from those encountered in oxides. For example the main group metal compounds and specially first row transition metal consist $[MN_3]^{n-}$ triangular anions, for example, Sr_6GaN_5, Ca_6AN_5 (A = Mn, Fe, Ga), and AE_3MN_3 (AE = Sr, Ba; M = Cr, Mn, Fe, Ga) and Ca_3AN_3 (A = V, Cr, Mn). These compounds confirm that Ga^{3+} may often be substituted for trivalent transition-metal cations [2–5].

Mallinson et al. [5] synthesized the two novel compounds having related structures, strontium gallium nitrides that contain $[GaN_3]^{6-}$ anions, which they described while introducing early transition metals into solution in alkaline earth sodium gallium melts and synthesize crystals of ternary and higher nitrides containing first row metals.

Recently, Hashimoto and Yamane [6] used Na flux method and synthesized a quaternary compound Ba–Ga–Si–N and obtained small amount of red transparent platelet single crystals of Ba_4GaN_3O in main product of yellow transparent granular single crystals of $Ba_3Ga_2N_4$ and calculated its structural properties. As there is no sufficient detail about electronic structure and spectroscopic properties of the reported compound, therefore we aimed to calculate the structural, electronic, and optical properties of tetrabarium gallium trinitride oxide (TGT) using the full potential linear augmented plane wave (FP-LAPW) method which proved to be one of the most precise method for electronic structure calculations [7,8] within the framework of the density functional theory (DFT). The rest of present paper is prearranged as follows. In Section 2, we present the computational details. The calculation results and discussions are given in Section 3. The conclusion is in Section 4.

2. Crystal structure and method of calculation

The crystallographic data of TGT oxide was taken from Hashimoto and Yamane [6] work. The TGT has chemical formula Ba_4GaN_3O which crystallizes in an orthorhombic cell with the space group *Pbca* (No. 61). TGT contains eight formula's per unit

* Corresponding author. Tel.: +420 777 083 956; fax: +420 386361219
E-mail address: sayaz_usb@yahoo.com (S.A. Khan).

http://dx.doi.org/10.1016/j.materresbull.2015.04.064
0025-5408/

cell as shown in Fig. 1. The experimental lattice parameters are $a = 7.8130$ Å, $b = 25.6453$ Å, $c = 7.9162$ Å.

All electron full potential linear augmented plane wave (FPLAPW) method within WIEN2K code [9] were used to calculate the electronic band structure, density of state, valence electron charge density along with optical properties of TGT. The exchange correlation functional was solved by Perdew, Burke, Ernzerhof Generalized gradient approximation (PBE-GGA) [10]. In recent literature this scheme shows good agreement with both experimental and theoretical data [11].

For convergence of energy eigenvalues the wave function in the interstitial regions were expended in plane waves (4 1 4 6 3) with cutoff $R_{MT}K_{max} = 7.0$. Where R_{MT} represent the muffin-tin (MT) sphere radius and K_{max} represent the magnitude of largest K vector. The selected R_{MT} are 2.39 a.u. for Ba and O atoms, 1.80 a.u. for Ga and 1.55 a.u. for N. The wave-function inside the sphere was expended up to $l_{max} = 10$ and Fourier expansion of the charge density was $G_{max} = 12\,(\text{a.u.})^{-1}$. The structure is optimized by minimizing of the forces that act on the atoms. The self-consistent calculations are supposed to be converged when the difference in total energy of the crystal did not exceed 10^{-5}Ryd for subsequent steps. The k-space integrations were done by using a modified tetrahedron integration scheme using 216 k points in irreducible Brillouin zone (IBZ) with $(17 \times 5 \times 16)$ Monkhorst–Pack grid [12]. The present calculations deal the core electrons fully relativistically, whereas scalar relativistic approximation was used for the valence states [13].

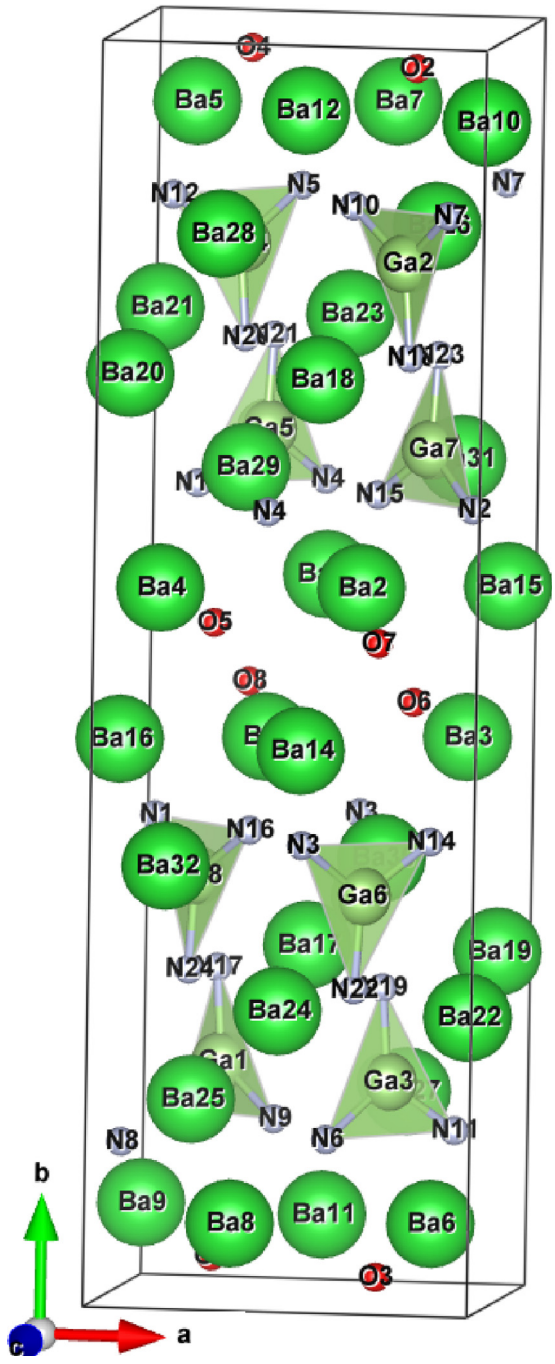

Fig. 1. Unit cells of TGT.

3. Result and discussion

3.1. Electronic band structure and density of state

The electronic band structure of TGT is calculated along high symmetry of the Brillouin zone (S–R–Z–Γ–Y–T) using PBE-GGA format as shown in Fig. 2. The calculated band structures of TGT expose a direct band gap of 1.38 eV around Γ point of the BZ. The angular momentum decomposition of the atoms projected density of states (DOS) make easy to identify the angular momentum character of a variety of structures of TGT. The total density of state inside a muffin-tin sphere for a single atom and its angular momentum are shown in Figs. 3 and 4 . The strong oscillations of the DOS plots were broadened by selecting Gauss-broadening factor with value of 0.003.

The low lying bands around −16.5 eV are mainly originated from O-s state. The next structure of the bands between −15.0 eV and −11.0 eV is fashioned by Ga-d, Ba-p and N-s states. The structures around −4.5 eV are formed by strong hybridization of Ga-s and N-s/p states. The O-p state mainly contributes in lower valence bands formation along with small part of N-p state. As one

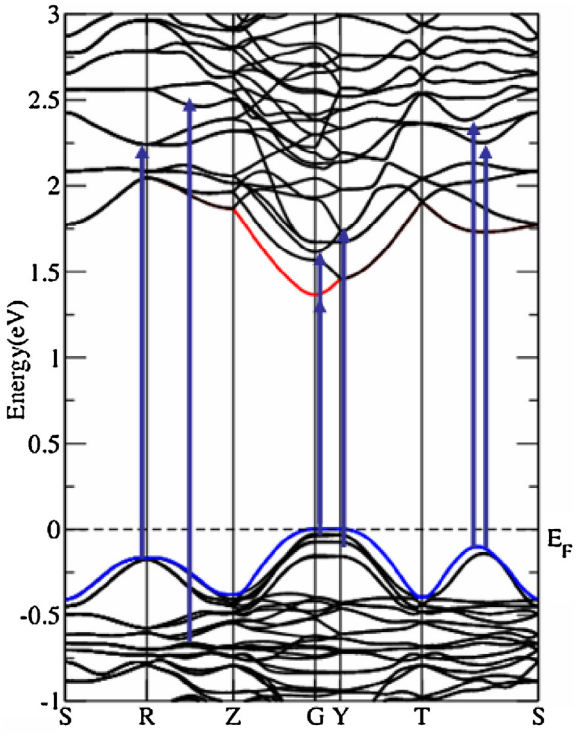

Fig. 2. Calculated band structure of TGT.

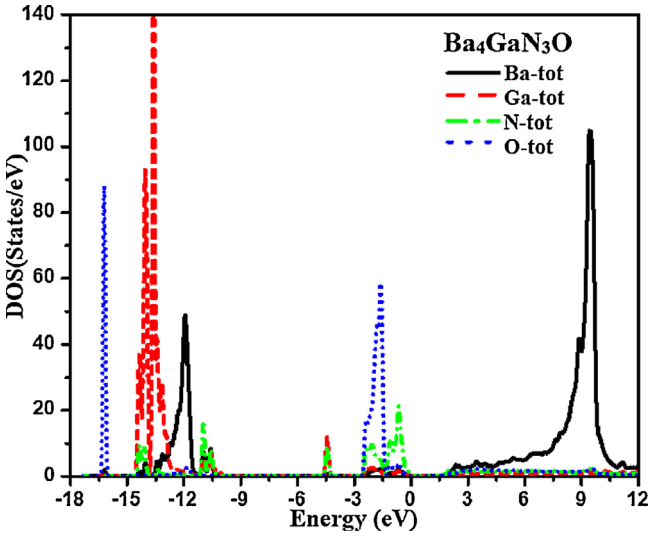

Fig. 3. Calculated total density of states (States/eV) of TGT.

move to higher energy (−1.4 eV) density of O-p state abruptly decreases from 7.3 to 0.1 states/eV and N-p state become dominant (2.5 states/eV) below Fermi level. Hence, N-p is more responsible for valence band formation. The conduction bands are formed by combination of N-p, Ba-d and negligible O-p states.

3.2. Electronic charge density

The accurate bonding nature of the material can be calculated from valence electron charge density (ECD) contour [14–16]. The calculated (ECD) plots show mix ionic-covalent nature of TGT as shown in Fig. 5. The scale shows the intensity of the charge density in which the red color shows the zero charge density while the blue color shows the maximum intensity. The Ga atom shares the charge with three N atoms form covalent bond. For verification of accuracy of bond nature one can use the Pauling scale of electro-negativity. According to Pauling scale if the electro-negativity difference is greater than 1.7, it shows the ionic nature while less than 1.7 show covalent nature of bond. The electro-negativity difference of the bonded atoms {(Ba–N = 0.9), (Ga–N = 1.6) and (Ba–N = 0.9)} clarify the dominant covalent and partially ionic nature of the reported bonds. In order to check the accuracy of the present calculation we compared the calculated bond lengths to the experimental results, listed in Table 1. Close agreement was found to the Hashimoto and Yamane [6] work.

3.3. Optical properties

The optical spectroscopy analysis of is a powerful tool to determine the overall band behavior of a solid. The band structure of the material is directly related to its complex dielectric function [17,18]. The energy eigenvalues and electron wave-functions which are natural output of the band structure calculation are necessary to calculate complex dielectric function $\varepsilon(\omega)$. The imaginary part of dielectric function can be described using the expression [19].

$$\varepsilon_2^{ij} = \frac{4\pi^2 e^2}{Vm^2\omega^2} \times \sum_{nn'\sigma} \langle kn\sigma|p_i|kn'\sigma\rangle \left\langle kn'\sigma|p_j|kn\sigma\right\rangle \times f_{kn}(1 - f_{kn'})\delta(E_{kn'} - E_{kn} - \hbar\omega) \quad (1)$$

where e and m represent charge and mass of electron and ω symbolize the electromagnetic radiation (EM) which strike the crystal volume (V) of the unit cell. The symbol p in bracket notation

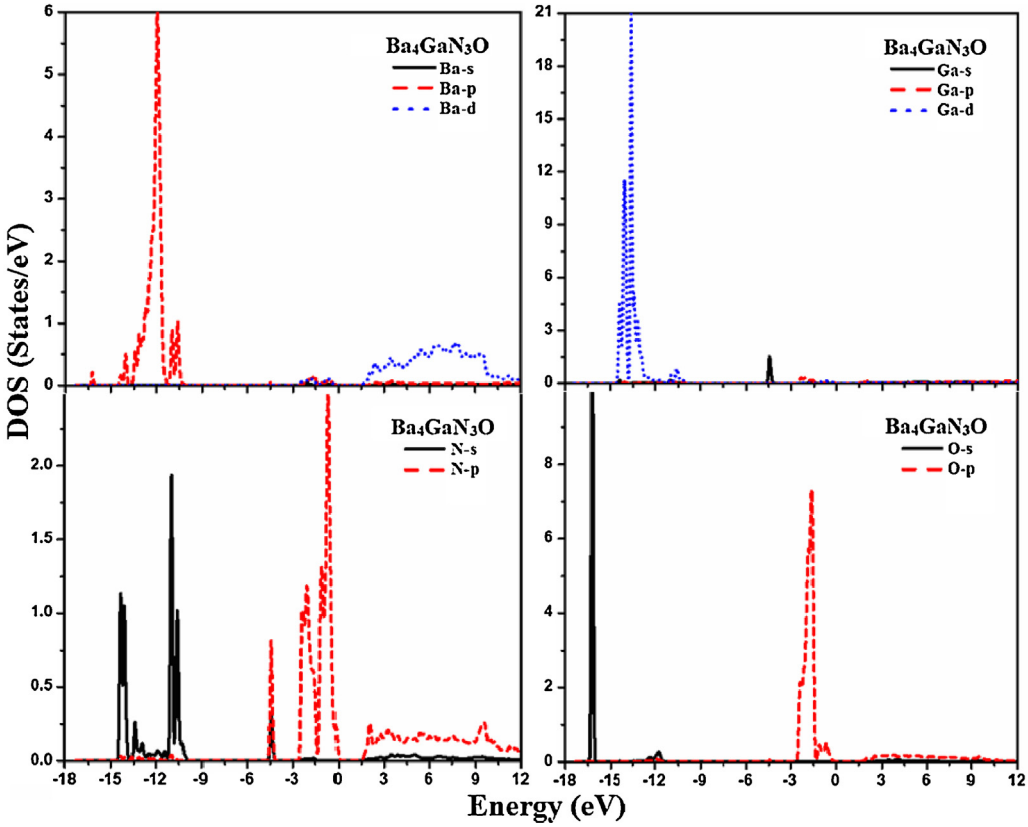

Fig. 4. Calculated partial density of states (States/eV) of TGT.

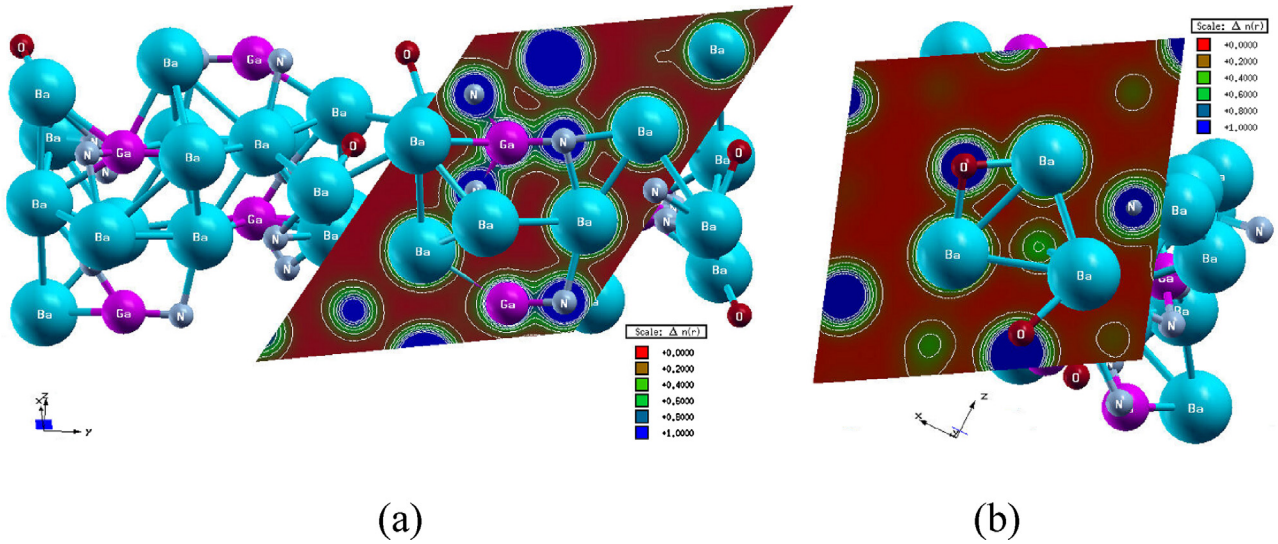

Fig. 5. Calculated valence electronic charge density plots of TGT. (For interpretation of the references to color in text, the reader is referred to the web version of this article.)

correspond to the momentum operator, the ket$|kn\sigma\rangle$ shows the crystal wave function with crystal momentum k and σ spin which correspond to the eigenvalue E_{kn}. The Fermi distribution function is symbolized by f_{kn} defines the counting of transition from occupied to unoccupied state and $\delta(E_{kn'} - E_{kn} - \hbar\omega)$ shows the condition for total energy conservation.

The crystal structure of TGT is orthorhombic having space group Pbca which allows three principal second order dielectric tensor components $\{\varepsilon^{xx}(\omega), \varepsilon^{yy}(\omega)$ and$\varepsilon^{zz}(\omega)\}$ along a, b and c crystallographic axis. The spectral peaks show electron dipole transitions from occupied bands to unoccupied bands. These spectral peaks can be identified using the critical points in the band structure, which are the points where the gradients of the two bands between which the transition occur are identical. The optical spectra of the imaginary part of the dielectric tensor components of TGT $\{\varepsilon_2^{xx}(\omega), \varepsilon_2^{yy}(\omega)$ and$\varepsilon_2^{zz}(\omega)\}$ are shown in Fig. 6(a). The TGT shows high transparency to the electromagnetic radiations in energy range between 0.0 eV and 1.38 eV. The threshold peak of the imaginary part emerges at about 1.38 eV that is related to the transition from the top of valence band (N-p state) to the bottom of conduction band (Ba-d). Rest of the electrons transition shown by arrows in Fig. 2 are also from N-p state to Ba-d and N-p state. The real part of dielectric function can be calculated from imaginary part using Kramer–Kronig relation [20].

$$\varepsilon_1(\omega) = 1 + \frac{2}{\pi} P \int_0^{\infty} \frac{\omega' \varepsilon_2(\omega')}{\omega'^2 - \omega^2} d\omega' \tag{2}$$

In the expression, P represents the principal value of integral. The real part of dielectric function is related to the electric polarizibilty of the material. The static values of dielectric tensor components were calculated. These values are presented in Table. 2. The uniaxial anisotropy (0.4842) among the dielectric tensor components were calculated with expression $\delta\varepsilon = \left[(\varepsilon_0^{\parallel} - \varepsilon_0{}^{\perp})/\varepsilon_0^{\text{tot}}\right]$ given in Ref. [21], which indicates a strong anisotropy among the three dominant dielectric tensor components $\{\varepsilon_1^{xx}(\omega), \varepsilon_1^{yy}(\omega)$ and $\varepsilon_1^{zz}(\omega)\}$ of TGT as shown in Fig. 6(b). One can note that a smaller energy optical gap correspond to larger $\varepsilon_1(0)$ value. In order to explain this phenomenon, Penn proposed a relation between $\varepsilon(0)$ and E_g, $\varepsilon(0) \approx 1 + (\hbar\omega_P/E_g)^2$known as Penn model [22]. Here, E_g is some kind of averaged energy gap which can be correlated to the real energy gap. It is obvious that E_g is inversely proportional to $\varepsilon(0)$. Consequently smaller E_g yields a larger value of $\varepsilon(0)$. Moreover both static values of real part of dielectric function and refractive indices are directly related through the $n(\omega) = \sqrt{\varepsilon_1(0)}$ shown in Table 2 which consequently show the accuracy of the performed calculations. We also calculated the static birefringence using the relation$\Delta n = n_e - n_0$. Where n_e and n_0 are the refractive indices of extraordinary and ordinary ray of polarized light. The birefringence is very important in the non-absorbing region below the gap [21]. The calculated static values of Δn for TGT are shown in Table 2. The calculated $\delta\varepsilon$ and Δn values show high effectiveness for second harmonic generation.

Fig. 6(c) shows the spectral components of the absorption coefficient. The two main peaks show maximum absorption around 6.0 eV and 20.0 eV. The spectral components of the absorption coefficient $I^{xx}(\omega)$, $I^{yy}(\omega)$ and $I^{zz}(\omega)$ exhibit a considerable anisotropy from 4.0 eV to 10.0 eV in first peak and from 14.0 eV to 24.0 eV in peak. The calculated dielectric tensor components of refractive indices are also related to the electric polarizability of the material as shown in Fig. 6(d). The refractive index of TGT

Table 1
Calculated bond lengths of tetrabarium gallium trinitride oxide (TGT).

Geometric parameters (Å)					
	Opt data[a]	Expt data		Opt data[a]	Expt data
Ba1–N1	2.792	2.675	Ba4–N1	3.319	3.231
Ga1–N2	1.920	1.908	Ba1–N2	3.079	2.998
Ga1–N3	1.908	1.876	Ba1–O1	2.747	2.999
Ga1–N1	1.957	1.924	Ba1–Ga1	3.328	3.246
Ga1–Ba1	3.328	3.246	Ba2–O1	2.555	2.683
Ga1–Ba3	3.755	3.364	N1–Ga1	1.957	1.924
Ba2–N1	2.899	2.991	N2–Ba4	2.767	2.675
Ba2–N2	2.653	3.158	N1–Ba3	2.896	2.914
Ba2–O1	3.089	3.184	N1–Ba2	2.899	2.991
Ba2–Ga1	3.327	3.340	N2–Ba2	2.653	2.687
Ba3–N3	2.727	2.730	N2–Ba4	2.793	2.862
N2–Ba1	3.089	2.998	Ba3–N3	2.770	2.764
N3–Ba4	2.716	2.661	Ba4–N2	2.767	2.862
Ba3–N1	2.896	2.914	N3–Ba3	2.727	2.730
O1–Ba2	2.555	2.683	Ba4–N3	2.716	2.661

Experimental data [6].
[a] Optimize data (PBE-GGA).

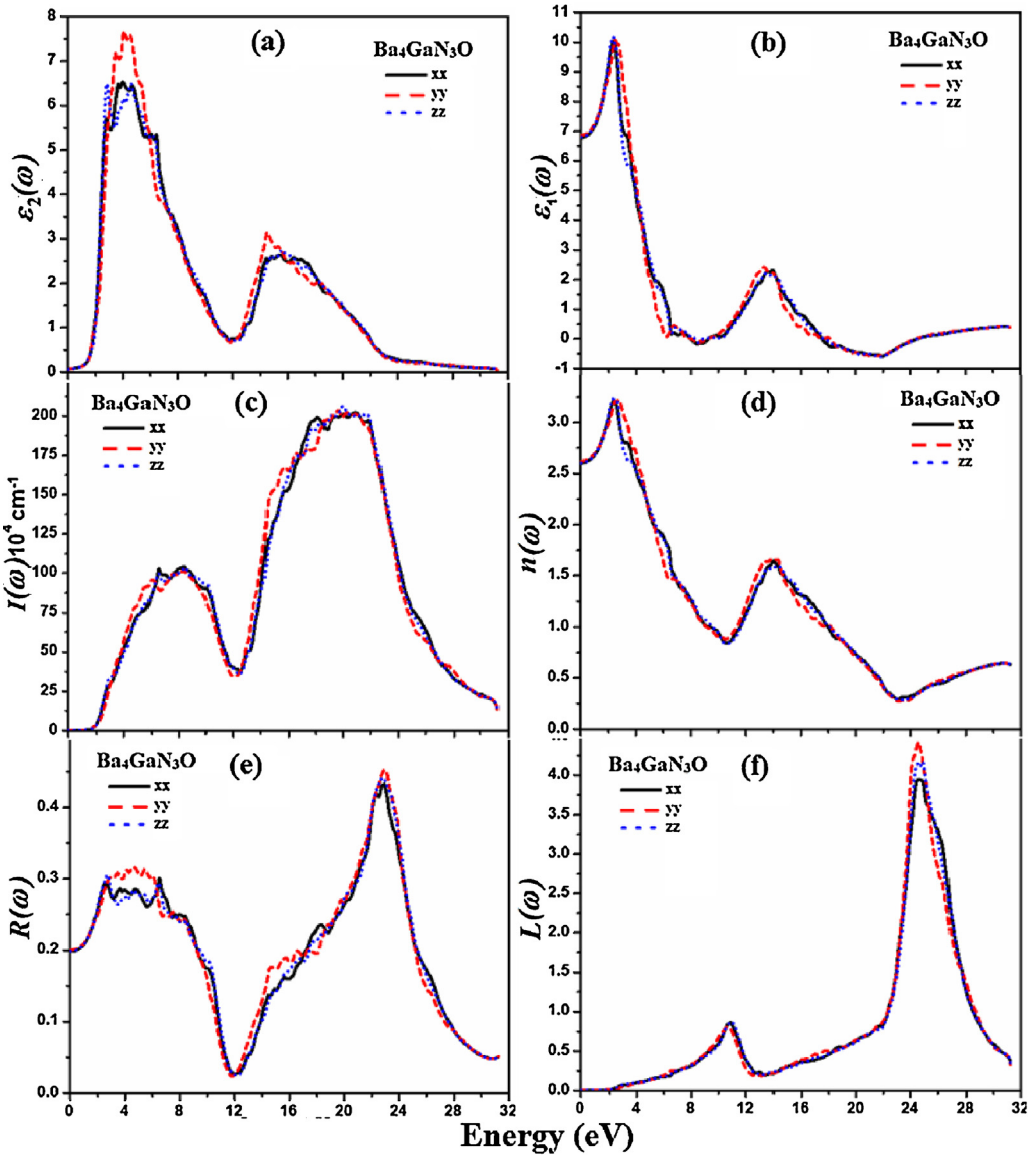

Fig. 6. (a) Calculated $\varepsilon_2^{xx}(\omega)$,$\varepsilon_2^{yy}(\omega)$ and $\varepsilon_2^{zz}(\omega)$ of TGT, (b) calculated $\varepsilon_1^{xx}(\omega)$, $\varepsilon_1^{yy}(\omega)$ and $\varepsilon_1^{zz}(\omega)$ of TGT, (c) calculated $I^{xx}(\omega)$, $I^{yy}(\omega)$ and $I^{zz}(\omega)$ of TGT, (d) Calculated $n^{xx}(\omega)$, $n^{yy}(\omega)$ and $n^{zz}(\omega)$ of TGT, (e) Calculated $R^{xx}(\omega)$, $R^{yy}(\omega)$ and $R^{zz}(\omega)$ of TGT, (f) calculated $L^{xx}(\omega)$, $L^{yy}(\omega)$ and $L^{zz}(\omega)$ of TGT.

Table 2
Calculated band gap and linear optical constants of Ba_4GaN_3O.

	Theoretical[a]	Experimental[b]
Volume (Å^3)	1584.16	1586.14
Density (Mg/cm^3)	5.675	5.671
E_g(eV)	1.379	
$\varepsilon_1^{xx}(0)$	6.782	
$\varepsilon_1^{yy}(0)$	6.862	
$\varepsilon_1^{zz}(0)$	6.790	
n^{xx} (0)	2.604	
n^{yy} (0)	2.619	
n^{zz} (0)	2.605	
$\delta\varepsilon$	0.484	
$\Delta n(0)$	−0.006	
ω_{pxx}	0.153	
ω_{pyy}	0.004	
ω_{pzz}	0.066	

[a] Present work.
[b] Theoritical work Ref. [6].

gradually increases and shows maximum value around 2.5 eV. As the energy of the incident radiation increases, there is an abrupt decrease in $n(\omega)$ which cross the unity around 9.0 eV and the phase velocity of monochromatic wave exceeds the velocity of light which leads to a controversy ($n = c/v$). On the other hand in dispersive medium, the wave propagate in form of wave packet having group velocity instead of phase velocity. The group velocity is related to phase velocity by expression $v_g = c/n$. According to this expression, v_g is always less than v. Though the transmitted signal $v > c$ the group velocity $v_g < c$ [23]. The dielectric tensor components of the reflectivity spectra {$R^{xx}(\omega)$, $R^{yy}(\omega)$ and $R^{zz}(\omega)$} are shown in Fig. 6(e). The static value of dielectric tensor components shows 2%, 3% and 4% of reflection for the components, respectively. There exists a considerable anisotropy among $R^{xx}(\omega)$, $R^{zz}(\omega)$ and $R^{yy}(\omega)$ around 4.0 eV and 16.0 eV. The material show maximum reflectivity of 46% around 23.0 eV. Fig. 6(f) represents the energy loss function $L(\omega)$ which describes the energy loss of fast electron traveling in the material. The sharp peaks produced in $L(\omega)$ around 10.5 and 25.0 eV are due to the plasma oscillation. The calculated plasma frequency of dielectric tensor components , ω_{pyy} and ω_{pzz}

around 10.5 eV are 0.1536, 0.004 and 0.066. This plasmon loss also cause decrease in reflectivity spectra.

4. Conclusion

In present work, we have selected to calculate the electronic band structure, valence electron charge density, total and partial density of states and optical properties of tetrabarium gallium trinitride oxide (TGT). All electron state-of-art FPLAPW as implemented in WIEN2k code in the framework of DFT, was used. The exchange correlation energy was solved using PBE-GGA functional. The strong hybridization of the orbitals confirms the dominant covalent nature of the bonds and provides the details about bands formation. The calculated electronic charge density plots confirmed covalent-ionic nature of the bond. The spectral peaks of imaginary part of dielectric function showed transition of electrons from occupied bands to unoccupied bands. The anisotropy (0.484) of the principal dielectric tensor components and birefringence (−0.006) were calculated. At 10.5 eV the behavior of the material change from linear to nonlinear as the $n(\omega)$ value cross the unity. The energy loss spectra show plasmon loss around 10.5 eV and 25.0 eV. The calculated the spectroscopic properties TGT show high effectiveness for optical devices.

Acknowledgments

The result was developed within the CENTEM project, reg. no. CZ.1.05/2.1.00/03.0088, co-funded by the ERDF as part of the Ministry of Education, Youth and Sports OP RDI program and, in the follow-up sustainability stage, supported through CENTEM PLUS (LO1402) by financial means from the Ministry of Education, Youth and Sports under the National Sustainability Programme I. MetaCentrum (LM2010005) and CERIT-SC (CZ.1.05/3.2.00/08.0144) infrastructures.

References

[1] Glen R. Kowach, H.Y. Lin, F.J. DiSalvo, J. Solid State Chem. 141 (1998) 1–9.
[2] S.J. Clarke, F.J. DiSalvo, Inorg. Chem. 36 (1997) 1143.
[3] L. Cario, Z.A. Ga'l, T.P. Braun, F.J. DiSalvo, B. Blaschkowski, H.J. Meyer, J. Solid State Chem. 162 (2001) 90.
[4] M.S. Bailey, F.J. DiSalvo, Dalton Trans. (2003) 2621.
[5] P.M. Mallinson, Z.A. Gál, S.J. Clarke, Inorg. Chem. 45 (2006) 419–423.
[6] T. Hashimoto, H. Yamane, Acta Cryst. E70 (2014) i28.
[7] S. Gao, Comput. Phys. Commun. 153 (2003) 190.
[8] K. Schwarz, J. Solid State Chem. 176 (2003) 319.
[9] P. Blaha, K. Schwarz, G.K.H. Madson, D. Kvasnicka, J. Luitz, WIEN2K, Technische Universitat Wien, Austria, 2001 ISBN: 3-9501031-1-1-2.
[10] J.P. Perdew, S. Burke, M. Ernzerhof, Phys. Rev. Lett. 77 (1996) 3865.
[11] K.M. Wong, S.M. Alay-e-Abbas, A. Shaukat, Y. Fang, Y. Lei, J. Appl. Phys. 113 (2013) 014304.
[12] H.J. Monkhorst, J.D. Pack, Phys. Rev. B 13 (1976) 5188–5192.
[13] K.M. Wong, S.M. Alay-e-Abbas, Y. Fang, A. Shaukat, Y. Lei, J. Appl. Phys. 114 (2013) 034901.
[14] R. Hoffman, Rev. Mod. Phys. 60 (1988) 601–628.
[15] C.D. Gellatt, A.R. Willaims Jr., V.L. Moruzzi, Phys. Rev. B 27 (1983) 2005–2013.
[16] A.H. Reshak, S.A. Khan, S. Auluck, RSC Adv. 4 (2014) 6957–6964.
[17] S.A. Khan, A.H. Reshak, Comput. Mater. Sci. 95 (2014) 328–336.
[18] A.H. Reshak, S.A. Khan, S. Auluck, RSC Adv. 4 (2014) 11967–11974.
[19] A. Delin, P. Ravindran, O. Eriksson, J.M. Wills, Int. J. Quantum Chem. 69 (1998) 349.
[20] F. Wooten, Optical Properties of Solids, Academic Press, New York, 1972.
[21] S.A. Khan, A.H. Reshak, Polyhedron 85 (2015) 962–970.
[22] D.R. Penn, Phys. Rev. B 128 (1962) 2093.
[23] M. Fox, Optical Properties of Solids, Oxford University Press, 2001.